Naval Research Laboratory
Washington, DC 20375-5320

NRL/MR/6410--97-8101

Computation of the 3-D Unsteady Flow Past Deforming Geometries

RAVI RAMAMURTI
WILLIAM C. SANDBERG

Center for Reactive Flow and Dynamical Systems
Laboratory for Computational Physics and Fluid Dynamics

RAINALD LÖHNER

The George Mason University
Fairfax, Virginia

October 20, 1997

19971121 101

DTIC QUALITY INSPECTED 3

Approved for public release; distribution is unlimited.

REPORT DOCUMENTATION PAGE

Form Approved
OMB No. 0704-0188

Public reporting burden for this collection of information is estimated to average 1 hour per response, including the time for reviewing instructions, searching existing data sources, gathering and maintaining the data needed, and completing and reviewing the collection of information. Send comments regarding this burden estimate or any other aspect of this collection of information, including suggestions for reducing this burden, to Washington Headquarters Services, Directorate for Information Operations and Reports, 1215 Jefferson Davis Highway, Suite 1204, Arlington, VA 22202-4302, and to the Office of Management and Budget. Paperwork Reduction Project (0704-0188), Washington, DC 20503.

1. AGENCY USE ONLY (*Leave Blank*)	2. REPORT DATE	3. REPORT TYPE AND DATES COVERED
	October 20, 1997	

4. TITLE AND SUBTITLE

Computation of the 3-D Unsteady Flow Past Deforming Geometries

5. FUNDING NUMBERS

6. AUTHOR(S)

Ravi Ramamurti, William C. Sandberg, and Rainald Löhner*

7. PERFORMING ORGANIZATION NAME(S) AND ADDRESS(ES)

Naval Research Laboratory
Washington, DC 20375-5320

8. PERFORMING ORGANIZATION REPORT NUMBER

NRL/MR/6410--97-8101

9. SPONSORING/MONITORING AGENCY NAME(S) AND ADDRESS(ES)

Naval Research Laboratory
Washington, DC 20375-5320

10. SPONSORING/MONITORING AGENCY REPORT NUMBER

11. SUPPLEMENTARY NOTES

*The George Mason University
Fairfax, VA

12a. DISTRIBUTION/AVAILABILITY STATEMENT

Approved for public release; distribution unlimited.

12b. DISTRIBUTION CODE

13. ABSTRACT (*Maximum 200 words*)

A 3-D incompressible unsteady flow solver based on simple finite elements with adaptive remeshing and grid movement for both moving and deforming surfaces is described. We demonstrate the combination of adaptive remeshing technique with the incompressible flow solver by computing the flow past an undulating eel in 2-D and past a swimming bluefin tuna in 3-D. It is clear that proper choice of the amplitude and frequency of undulation is necessary for positive thrust production in the eel. Unsteady flow of the swimming tuna with caudal fin oscillation and quasi-steady state flow at several caudal fin positions are computed. Comparison of these results show that the unsteady flow is considerably different in both magnitude and trend suggesting that unsteady flow about moving deforming bodies is not amenable to spatial decomposition or temporal, quasi-steady approximations.

14. SUBJECT TERMS

Deforming geometry
Adaptive remeshing
Incompressible flow
Tuna

15. NUMBER OF PAGES

24

16. PRICE CODE

17. SECURITY CLASSIFICATION OF REPORT	18. SECURITY CLASSIFICATION OF THIS PAGE	19. SECURITY CLASSIFICATION OF ABSTRACT	20. LIMITATION OF ABSTRACT
UNCLASSIFIED	UNCLASSIFIED	UNCLASSIFIED	UL

NSN 7540-01-280-5500

Standard Form 298 (Rev. 2-89)
Prescribed by ANSI Std 239-18
298-102

DTIC QUALITY INSPECTED 3

CONTENTS

Computation of the 3-D Unsteady Flow Past Deforming Geometries

1. INTRODUCTION

The graceful motions of swimming fish, which appear almost effortless, have fascinated people for thousands of years, dating at least back to Aristotle, and possibly earlier, according to Lindsey [1]. In recent years, since the early 1970's, there has been increased experimental and analytical investigation of the physiology, biomechanics, and hydrodynamics of fish propulsion, for the purposes of quantifying the energy budget and actual swimming speeds for a variety of fish propulsive modes. These modes were classified by Breder [2] in 1926 and characterized steady forward swimming according to the occurrence and extent of body undulations, fin oscillations, and combinations of the two. For example the eel generates thrust via undulatory motion, while the tuna produces thrust almost exclusively through the oscillation of its lunate tail, or caudal fin. Webb [3,4], who has studied the morphologic adaptations of fish for optimized locomotion, characterizes the tuna as a cruising specialist that has adapted for long distance steady swimming. Since the tuna body is relatively free from undulation it is an excellent case to examine analytically. The traditional hydrodynamics methods of slender body theory and elongated body theory unfortunately do not apply to the lunate fin of the tuna, as is discussed in detail by Yates [5], thus necessitating the use of unsteady lifting wing theories, which themselves require a number of simplifying assumptions to be made. Only recently has a capability for computing three-dimensional, unsteady incompressible flow over a changing geometry become available [6]. In that work, the flow field generated during a torpedo launch from a submarine was computed. In this paper we describe the extension of that work to carry out a direct computation, making no geometric simplifications, of the unsteady flow past geometries which are themselves varying in time. In particular, we describe the computation of unsteady flow past a tuna, including the oscillatory caudal fin motion with its associated surface deformation. We also describe the computation of the time variation of the pressure distribution over both surfaces of the caudal fin, as well as the body and the integration over all surfaces to obtain the unsteady thrust. This is the first such three-dimensional incompressible flow, unsteady thrust computation for a deforming body that we are aware of.

2. THE FLOW SOLVER

The governing equations employed are the incompressible Navier-Stokes equations in an Arbitrary Lagrangian Eulerian (ALE) formulation which are written as

$$\frac{\partial \mathbf{v}}{\partial t} + \mathbf{v}_a \cdot \nabla \mathbf{v} + \nabla p = \nabla \cdot \sigma \ , \tag{1a}$$

$$\nabla \cdot \mathbf{v} = 0 \ , \tag{1b}$$

Manuscript approved September 9, 1997

where p denotes the pressure, $\mathbf{v}_a = \mathbf{v} - \mathbf{w}$ the advective velocity vector (flow velocity $\mathbf{v}$ minus mesh velocity $\mathbf{w}$) and both the pressure p and the stress-tensor σ have been normalized by the (constant) density ρ, are discretized in time using an implicit timestepping procedure. It is important that the flow solver be able to capture the unsteadiness of a flow field if such exists. The present flow solver is built as time-accurate from the onset, allowing local timestepping as an option. The resulting expressions are subsequently discretized in space using a Galerkin procedure with linear tetrahedral elements. In order to be as fast as possible, the overhead in building element matrices, residual vectors, etc. should be kept to a minimum. This requirement is met by employing simple, low-order elements that have all the variables (u,v,w,p) at the same location. The resulting matrix systems are solved iteratively using a preconditioned gradient algorithm (PCG). The preconditioning is achieved through linelets [7]. The flow solver has been successfully evaluated for both 2-D and 3-D, laminar and turbulent flow problems by Ramamurti *et al.* [8,9]. The flow solver was also parallelized in order to improve its efficiency and portability to various supercomputer architectures. The parallelized grid generation and flow solver codes have been run on Intel iPSC/860, IBM SP-2 and CRAY C-90.

3. RIGID BODY MOTION

In order to fully couple the motion of rigid bodies with the hydrodynamic or aerodynamic forces exerted on them, consistent rigid body motion integrators must be developed. The governing equations of motion for rigid bodies [10] and for multiple bodies in relative motion [11] are well known. In the present work the pressure distribution on the surface is integrated to compute forces and moments at each time step and the equations of motion are advanced in time to produce self-consistent trajectories. A more detailed description of the equations and the incorporation of the rigid body motion in the numerical scheme for solving the fluid flow are described in [6].

4. GRID GENERATION, GRID MOTION, AND ADAPTIVE REMESHING

In order to carry out computations of the flow about oscillating and deforming geometries one needs to describe grid motion on a moving surface, couple the moving surface grid to the volume grid, and describe the remeshing of the volume grid in proximity to the moving surface. A representative application requiring these gridding capabilities is the computation of the vorticity shedding from the edges of oscillating foils, such as the tuna caudal fin which is described below. It is also essential for computing the flow past objects which are both accelerating and deforming. In deformations, the surface motion may be severe, leading, in the absence of remeshing, to distorted elements which in turn lead to poor numerical results. If the bodies in the flow field undergo arbitrary movement, a fixed mesh structure will lead to badly distorted elements. This means that at least a partial regeneration of the computational domain is required. On the other hand, if the bodies move through the flow field, the positions of relevant flow features will change. Therefore, in most of the computational domain a new mesh distribution will be required. One approach to solve these problems is to regenerate the whole computational domain adaptively, taking into consideration the current flow field solution. A typical simulation where bodies undergo severe motion typically requires hundreds of remeshings. It is thus clear that a fast reliable regridding capability is essential. In order to generate or regenerate a mesh reliably and quickly, we use the advancing front technique [12,13].

The use of optimal data structures, filtering of points and faces and automatic reduction of unused points along the advancing front has increased the speed of the grid generation process [6].

Currently, the advancing front algorithm constructs grids at a rate of 60,000 tetrahedra per minute for very small grids to 80,000 tetrahedra per minute for large grids on the CRAY-C90.

Our earlier simulations of two-body dynamics, where the two bodies were in close proximity, revealed that badly distorted elements occurred more often than expected. Given the relatively high cost of global remeshing, we explored the idea of local remeshing in the vicinity of the elements that became too distorted. In the local remeshing process the badly distorted elements and the elements that surround it are removed. Then, a new mesh is generated in the holes left by the removal of these elements. This is a fast process and takes 5-6 times less CPU time compared to global remeshing.

The identification of the region of moving elements and the mesh movement algorithm to be employed are also important from the point of view of mesh distortion and remeshing requirements. These are also discussed in detail in [6].

The capability to adaptively remesh and to selectively move the mesh enables one to describe the evolution of the surface deformation of objects such as air bags, parachutes, flexible tubing, living organisms such as flying birds and swimming fish, and human organs dynamics such as the flow in blood vessels and through the heart. We have chosen for this initial computation, a swimming fish. We have chosen this application for two reasons: 1.) An accurate specification of a realistic geometry was readily available, and 2.) The geometry has immediate practical implications for the design of submarines and other undersea vehicles. The geometry selected was that of the bluefin tuna. The tuna is of particular interest for naval applications since it is reported [3] to swim primarily via oscillation of the caudal (tail) fin, while most other fish use primarily undulatory motion of the body to generate propulsive thrust and maneuvering forces. The maneuvering of a submarine via stern plane oscillation is clearly analogous to the tuna caudal fin swimming mode. Recent experimental work at M.I.T. [14] on robotic tuna swimming has shown that undulatory motion coupled with properly phased caudal fin oscillation leads to drag reduction. We, however, have chosen not to incorporate body undulation in our computations since our primary motivation here is to demonstrate a capability for computation of unsteady forces on moving vehicle control surfaces, not to investigate the dynamical processes of vorticity control on actual tuna swimming. It is planned to incorporate body undulation in subsequent computations where vorticity dynamics will be the focus. As an initial step, prior to the 3-D computation on the tuna, several 2-D computations were carried out. These computations were aimed at computing the time-varying pressure distribution over an undulating surface, which was chosen to resemble that of an eel.

5. NUMERICAL EXAMPLES

5.1 2-D Undulatory Motion

In order to observe the process of longitudinal force generation by body undulation, 2-D computations of a deforming surface were carried out. The computations were performed primarily to test the coupled rigid body motion with the adaptive remeshing flow solver. Therefore the parameters were not chosen to correspond to specific cases of swimming by objects such as snakes or eels. Furthermore, any such comparisons made to real swimming creatures can only be qualitative since the computations are 2-D.

The body undulation was prescribed as a sinusoidal wave traveling from the head to tail as follows:

$$y = Asin\left\{2\pi(tf - \frac{x}{\lambda})\right\} \tag{2a}$$

The amplitude A is given by

$$A = \begin{cases} 0, & x < x_0, \\ A_{max}\ B(x), & x_0 < x < x_1 \text{ and} \\ A_{max}, & x > x_1. \end{cases} \tag{2b}$$

where A_{max} is the maximum amplitude, $B(x)$ is a blending function in the region x_0 to x_1, t is the time, f is the frequency and λ is the wavelength of the traveling wave.

Several computations were performed by varying the traveling wave speed and the amplitude of the wave. The computational grid, Fig. 1, shows adaptation to the body motion where 8 layers of elements that surround the surface move with it rigidly. In all the cases studied, the frequency f was maintained to be 1.5 Hz.

Case 1: The first simulation was performed with $\lambda = 1.0\ L$, $A_{max} = 0.1\ L$, where L is the length of the object. The variation of the thrust and the side force with time is shown in Fig. 2a. The mean thrust in this case is 0.0495 directed towards the head.

Case 2: Next, the wavelength of the traveling wave λ was decreased to 0.5 L while keeping $A_{max} = 0.1\ L$. The variation of the force components are shown in Fig. 2b. The mean thrust in this case is 0.047 directed towards the tail. This is due to the cancellation of the pressure force in the region of the tail which is responsible for a major contribution to the thrust.

Case 3: With A_{max} still held at 0.1 L, λ is increased to 1.25. The mean thrust is observed to increase to 0.0817, directed towards the head. The force component variation is shown in Fig. 2c.

Case 4: Finally with λ held fixed at 1.25 L, the maximum amplitude, A_{max}, was increased to 0.2 L. In this case, the mean thrust increased to 0.33 directed toward the head. The history of force components is shown in Fig. 2d. Figure 3 shows the instantaneous pressure distribution for this case.

One conclusion which can be drawn from these computations is that the adaptive remeshing and grid motion algorithms are sufficiently robust to compute the time-varying flow about this simple deforming surface for all frequencies of interest. It is also clear that the amplitude and frequency of undulation must be chosen properly to result in forward thrust. This is of course well known but it is nevertheless encouraging that our simple 2-D computations give results consistent with experimental observations of the anguilliform motion swimming eels [3] which show one or more wavelengths of large amplitude along the length of the body. Having demonstrated a capability to compute the flow past a 2-D deforming surface, we next proceeded to a 3-D deforming surface including fin oscillation.

5.2 3-D Deforming Body With Fin Oscillation

The surface definition and coordinate system for force computations is shown in Figure 5. The geometry is that of a bluefin tuna. As mentioned earlier, we intentionally selected the tuna since it is classified as a thunniform swimmer. That is, its primary means of thrust generation is from cadual fin oscillation rather than body undulation. The motion of the caudal fin was prescribed as follows:

$$z = A\sin(\omega t)\frac{(x - x_0)^2}{(x_1 - x_0)^2}, \tag{3}$$

where A is the amplitude of the motion at the tip of the caudal fin, ω is the angular frequency, x_0 is the location of the peduncle, which is the smallest part of the body where the caudal fin begins, and x_1 is the location of the tip of the caudal fin. The motion is shown in Fig. 4. The frequency of the caudal fin oscillation was chosen to be 12.5Hz as suggested by [15]. The mean line is prescribed as a parabolic arc from the peduncle so as to maintain C_1 (slope) continuity throughout the entire body. This also implies that the caudal fin must deform during the motion.

Several steady state solutions were obtained at various caudal positions during one quarter of a cycle. Forces generated by the caudal fin and the body were computed. Unsteady flow was computed for 3 cycles and the results compared with the steady-state one quarter cycle data.

Since our main purpose in this work was to demonstrate the capability of the code to compute the unsteady flow about deforming geometries it is sufficient, and considerably faster and thus cheaper, to consider the fluid as inviscid. An inviscid flow will require a much coarser grid, which translates to fast turnaround.

The speed of the tuna was chosen to be 10 $L/sec.$ [15], which is at the high end for fast cruising and feeding activity. First a steady state solution was obtained. Figure 6 shows the convergence history of pressure. It can be seen that convergence by almost 4 orders of magnitude on the residual error in the pressure equation is achieved in 750 iterations.

Using the steady flow field as the initial condition, the unsteady flow was computed for 3 cycles of the caudal fin oscillation. The time step $\Delta t = 10^{-4}$ was employed throughout and the entire unsteady computation was performed in 2400 steps. The grid for this computation consisted of approximately 52K points and 262K tetrahedra. 161 local remeshings and only 1 global remeshing occurred during the simulation. This is a very encouraging result that indicates that significant grid deformation which required remeshing was localized in small regions of the domain. The total computational time for this computation was approximately 12 CPU hours on a CRAY C-90. The time taken for advancing the flow 1 timestep was 17 seconds, the time for 1 local remeshing was 38 secs. and the time for 1 global remesh was 300 secs.

The time variation of the force components for the first 3 cycles is shown in Fig. 7. Notice that the direction of positive thrust is $-x$. This shows, not unexpectedly, that the thrust developed by the caudal fin motion is not quite sufficient to balance the nearly constant form drag on the body. The selected combination of flow speed, caudal fin frequency and amplitude of oscillation, and the

total exclusion of body undulation are no doubt responsible. It is perhaps worth repeating at this point that the intent of this work was **not** to compute the total force on a swimming fish for use in the analysis of fish dynamics. The fish is merely a convenient geometry with practical naval implications. An unsteady flow computation for a deforming geometry must have as a *sine qua non*, the capability for computation of the unsteady flow as the body is **continuously** deforming. We therefore intentionally excluded body undulation and viscous action from the present computations and thus would not expect to compare the results to any experimental fish data. We have demonstrated in this work the success of the method in accurately describing the deforming geometry and self-consistently computing the flow about it. This is particularly important for any bodies in motion as is vividly shown in Figure 8. Figure 8 shows the effect of the caudal fin position on the force components, both for the steady and unsteady simulations. It is clear that the results of the steady state simulation agree in neither the magnitude nor the trend with the variation of the forces seen in the unsteady simulation results. It is traditional to analyze the forces of moving control surfaces by computing the force and moment on the foil at successive positions through its complete cycle. The traditional approach is obviously not including the dynamics of the unsteady flow, which is the total flow associated with both the upstream unsteady pressure distribution variations caused by the moving or deforming surface and the unsteady flow about the continuously moving surface itself. Our results indicate that the flow field must be treated in its entirety and it is not amenable to spatial decomposition or temporal, quasi-steady approximations. Figures 9 and 10 emphasize this finding. They show the differences in the surface pressure distribution between the steady state and unsteady computation on the pressure and suction sides of the caudal fin, respectively. The minimum pressure in the unsteady computation is lower for all the three instants of time. The maximum pressure which occurs at the leading edge of the fin remains almost unchanged. In the steady state computations, Figs. 9a-c and 10a-c, the pressure contours are symmetric about the 'centerline' of the fish whereas the unsteady computations result in a higher pressure on the lower side of the peduncle. Figure 11 shows the surface pressure distribution at the end of 3 cycles. The high pressure regions in this case are near the mouth, the leading edges of the fins and near the gill. The velocity vectors on the surface, Fig. 12, show a low velocity region extending from the mouth to the tail along the centerline. We believe this is due to the fixed open mouth geometry. Since the fish mouth is not always open but is opening and closing, the low velocity regime does not persist but is rather more intermittent. We chose, again to avoid unnecessary complexity for our purpose, not to include opening and closing of and flow through the mouth and gills, although the code has the capability to do this. The magnitude , extent, and time variation of the leading high pressure region would clearly be altered were this to be done. A small recirculation region is also evidenced near the peduncle region. This could actually occur due to the corner flow that is set up at the maximum amplitude of oscillation and has potential for practical consequences in the selection of control surface oscillation strategies.

Recently, new data on swimming tuna has become available. Dewar and Graham [16] observed that for a tuna of approximately 14 inches in length, the mean swimming velocity is approximately 1 L/sec and the corresponding mean frequency of the caudal fin oscillation is approximately 2 Hz. We have also carried out computations for these parameter values. First a steady state solution was obtained. With the steady state solution as the initial condition, the unsteady simulation was performed. Figure 13a shows the time history of the force component in the x direction for two cycles of the caudal fin oscillation. The drag produced by the body up to the peduncle region remains almost constant at approximately 5.95lbs. The thrust produced by the caudal fin, Fig 13b, shows a sinusoidal variation, with a significantly smaller amplitude compared to the previous

simulation. This is due to the combination of the swimming speed and the frequency of oscillation. The total force of nearly 0.4lbs, from Fig. 13a, is again in the positive x direction, indicating that the body drag still overwhelms the thrust produced by the caudal fin oscillation. As mentioned before, the drag on the body is mainly due to the open mouth configuration. Hence, the drag due the mouth region was computed separately. It is approximately 5.3lbs. This amount was subtracted from the total force to give a corrected total force, which is shown in Fig. 13a. The result is a positive thrust of approximately, 4.9lbs. These computations indicate that a closed mouth configuration is necessary if true swimming dynamics computational investigations are desired.

6. CONCLUSIONS

A new, 3-D incompressible unsteady flow solver based on simple finite elements with adaptive remeshing and grid movement for both moving and deforming surfaces has been developed. The main algorithmic ingredients were described in this paper. We have demonstrated how the combination of adaptive remeshing techniques, an implicit incompressible flow solver for transient problems with moving grids, and integrators for body motion allows the simulation of fully coupled fluid-deforming body interaction problems of arbitrary geometric complexity in three dimensions, which geometry can be both *moving and simultaneously deforming.* The demonstration computations on the geometry of the bluefin tuna showed that the code can accurately describe moving and deforming surfaces and compute the unsteady flow about those surfaces. The results of the unsteady computations were found to be considerably different in both magnitude and trend from the results from steady computations. The results suggest that the unsteady flow about moving, deforming geometries is not amenable to spatial decomposition or temporal, quasi-steady approximations.

Acknowledgments

This work was supported by the Office of Naval Research through the NRL project on Unsteady Flows Past Deforming Bodies. Computations were carried out on the Cray C-90/16 at the Army Corps of Engineers Waterways Experiment Station (CEWES) under a computer grant from the DoD High Performance Computing Modernization Program Office (DoDHPCMO).

7. REFERENCES

1. Lindsey, C.C., "Locomotion," in *Fish Physiology*, **7**, ed. W.S. Hoar and D.J. Randall, Academic Press, 1978.
2. Breder, C.M., "The Locomotion of Fishes," *Zoologica*, **4**, pp. 159-256, N.Y., 1926.
3. Webb, P.W., "Form and Function in Fish Swimming," *Scientific American*, **251**, (1), 72, 1984.
4. Weihs, D. and Webb, P.W., "Optimization of Locomotion," in *Fish Biomechanics*, ed. P.W. Webb and D. Weihs, Praeger Scientific, 1983.
5. Yates, P.W., "Hydromechanics of Body and Caudal Fin Propulsion," in *Fish Biomechanics*, *ibid.*
6. R. Ramamurti, R. Löhner and W.C. Sandberg, "Simulation of a Torpedo Launch Using a 3-D Incompressible Finite Element Solver," *AIAA-95-0086*, Washington, D.C., 1995.
7. Martin, D. and Löhner, R., "An Implicit Linelet-Based Solver for Incompressible Flows," *AIAA-92-0668*, Washington, D.C., 1992.

8. Ramamurti, R. and Löhner, R., "Evaluation of an Incompressible Flow Solver Based on Simple Elements," *Advances in Finite Element Analysis in Fluid Dynamics*, FED Vol. 137, Editors: M.N. Dhaubhadel et al., ASME Publication, New York, pp. 33-42, 1992.
9. Ramamurti, R., Löhner, R. and Sandberg, W.C., "Evaluation of a Scalable 3-D Incompressible Finite Element Solver," *AIAA-94-0756*, Washington, D.C., 1994.
10. Meirovitch, L., "Methods of Analytical Dynamics," McGraw-Hill, New York, 1970.
11. Sandberg, W.C., "The Estimation of Ship Motion Induced Loads," 4th Ship Technology and Research Symposium, *SNAME*, pp. 347-351, 1979.
12. Löhner, R. and Parikh, P., "Three-Dimensional Grid Generation by the Advancing Front Method," *Int. J. Num. Meth. Fluids* 8, pp. 1135-1149, 1988.
13. Peraire, J., Morgan, K. and Peiro, J., " Unstructured Finite Element Mesh Generation and Adaptive Procedures for CFD," AGARD-CP-464, 18, 1990.
14. Triantafyllou, M.S., Barrett, D.S., Yue, D.K.P., Anderson, J.M., Grosenbaugh, M.A., Streitlien, K. and Triantafyllou, G.S., "A New Paradigm of Propulsion and Maneuvering for Marine Vehicles," *SNAME Transactions*, 1996.
15. Wardle, C.S., "Limit of Fish Swimming Speed," *Nature*, **255**, 725-727, 1975.
16. Dewar, H. and Graham, J.B., "Studies of Tropical Tuna Swimming Performance in a Large Water Tunnel," *J. Exp. Biol.* **192**, 45-59, 1994.

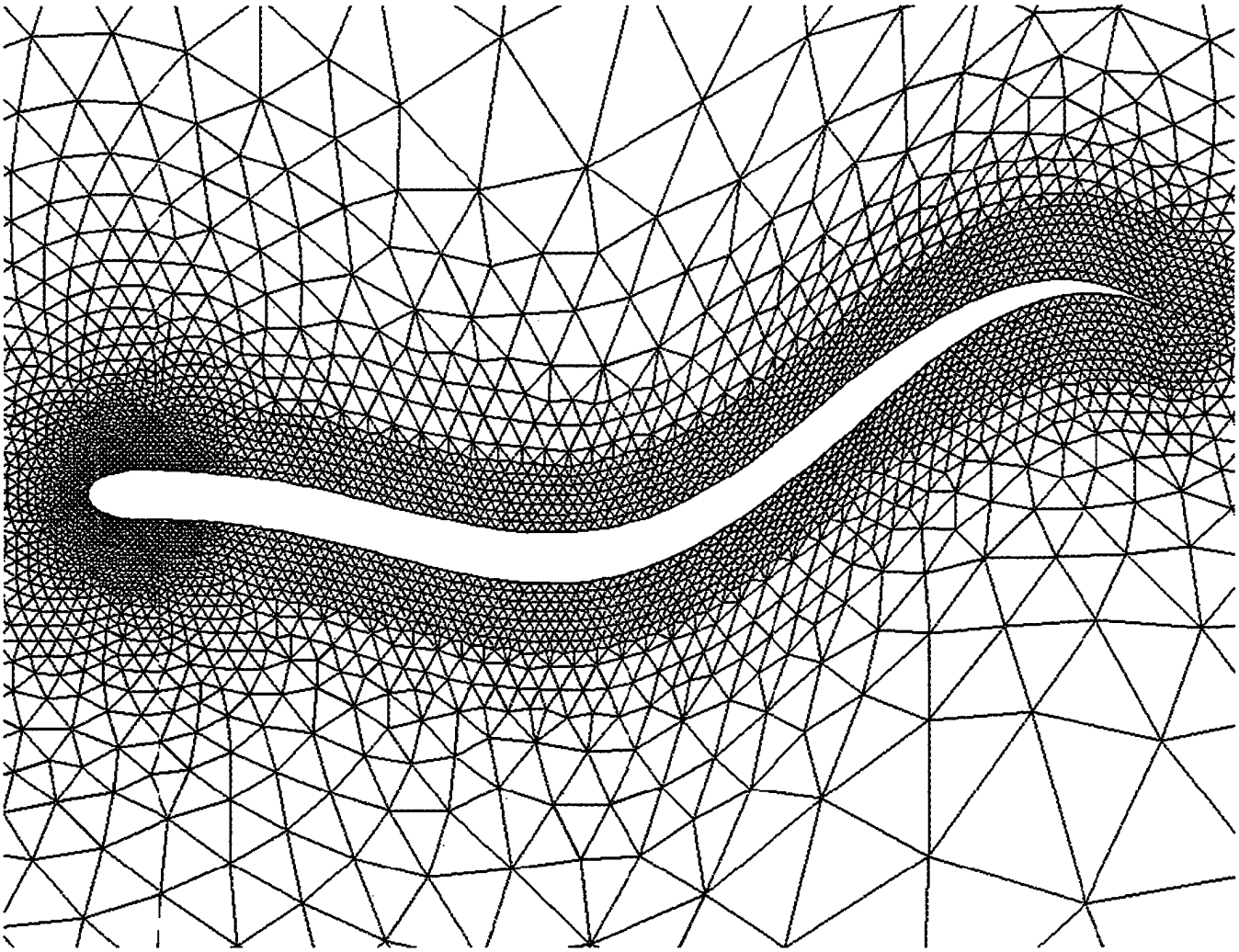

Fig. 1. Adapted Mesh About an Undulating Eel, nelem= 9,792, npoin= 5,091

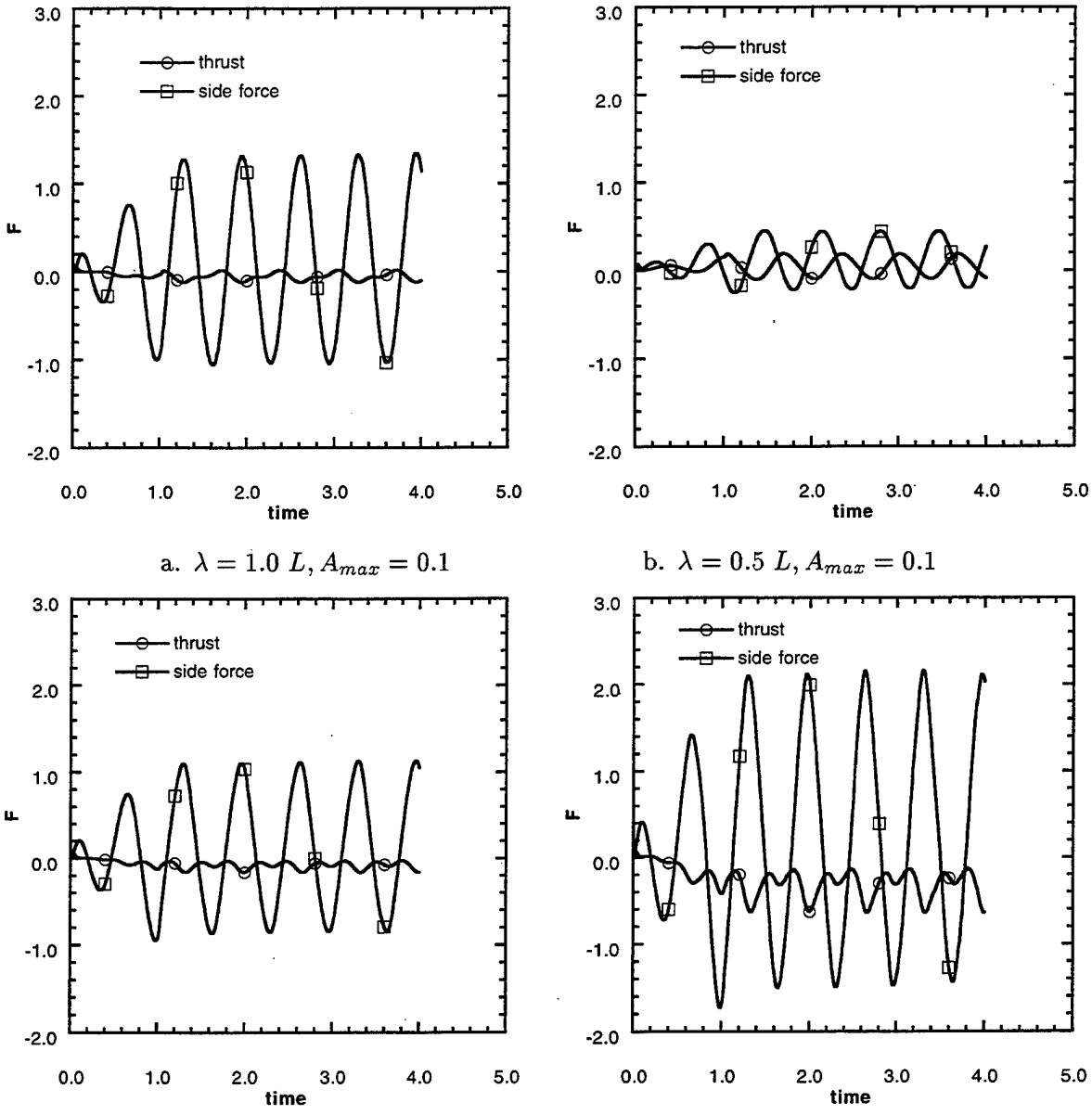

a. $\lambda = 1.0\ L, A_{max} = 0.1$

b. $\lambda = 0.5\ L, A_{max} = 0.1$

c. $\lambda = 1.25\ L, A_{max} = 0.1$

d. $\lambda = 1.25\ L, A_{max} = 0.2$

Fig. 2. Time History of Force on an Undulating Eel

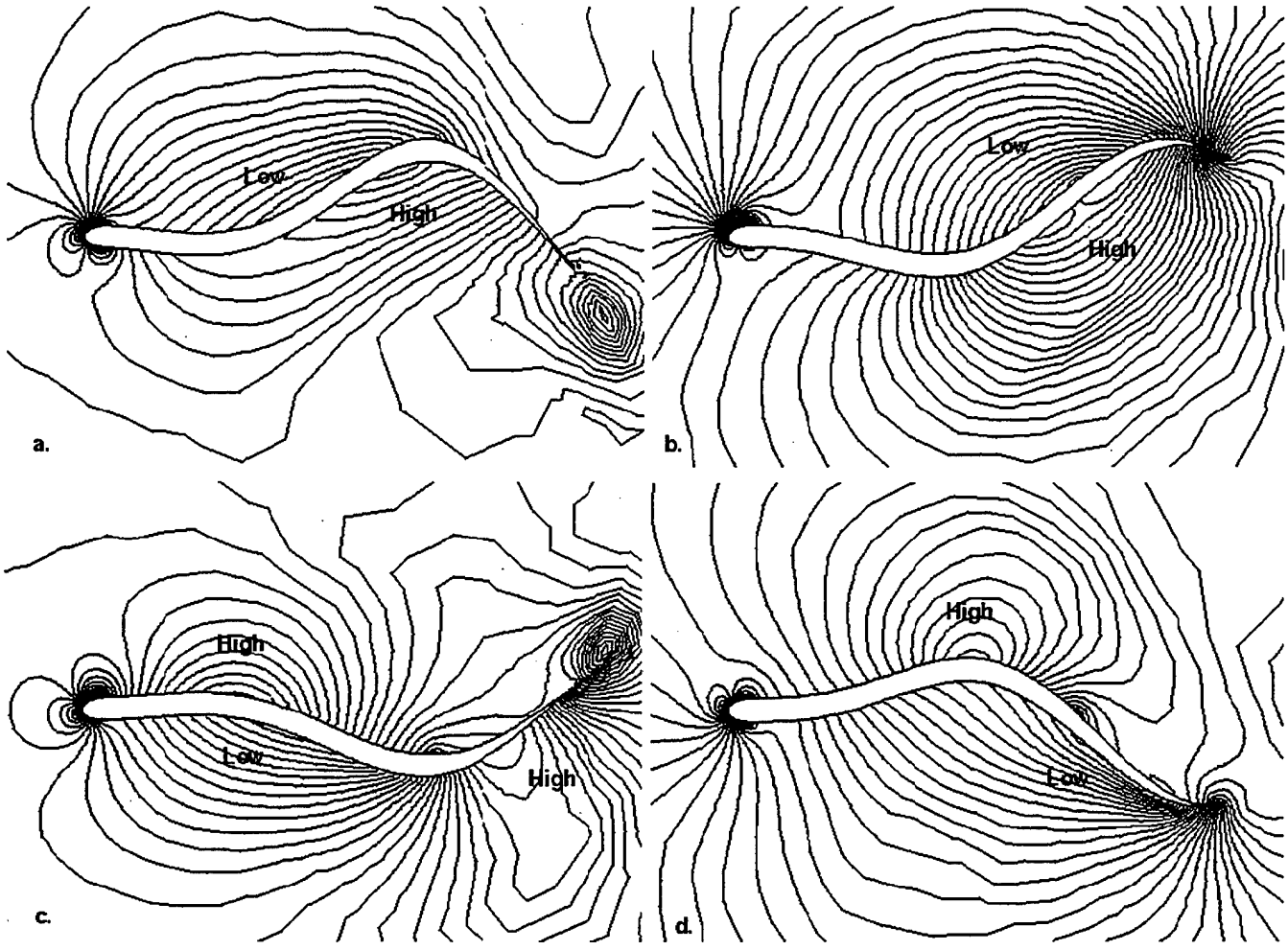

Fig. 3. Pressure Distribution on Undulating Eel, $\lambda = 1.25\ L, A_{max} = 0.2$

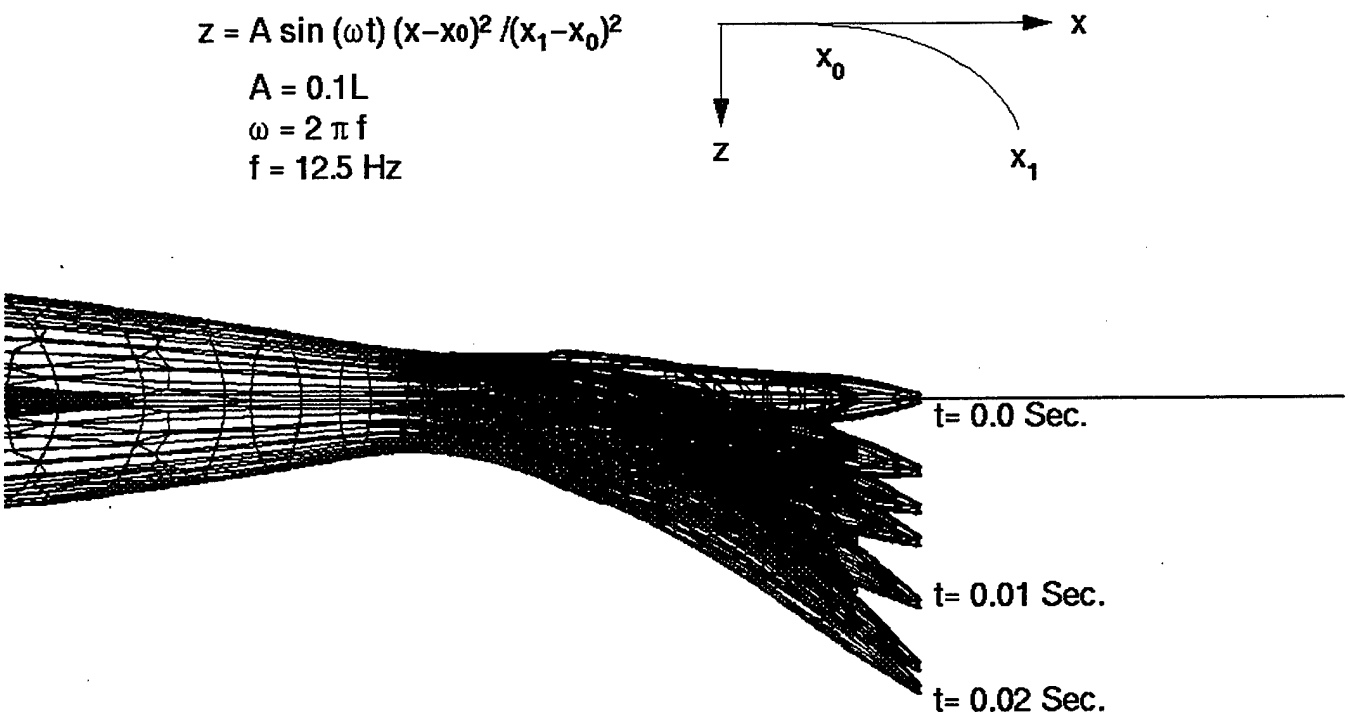

Fig. 4. Position of Caudal Fin at Various Times

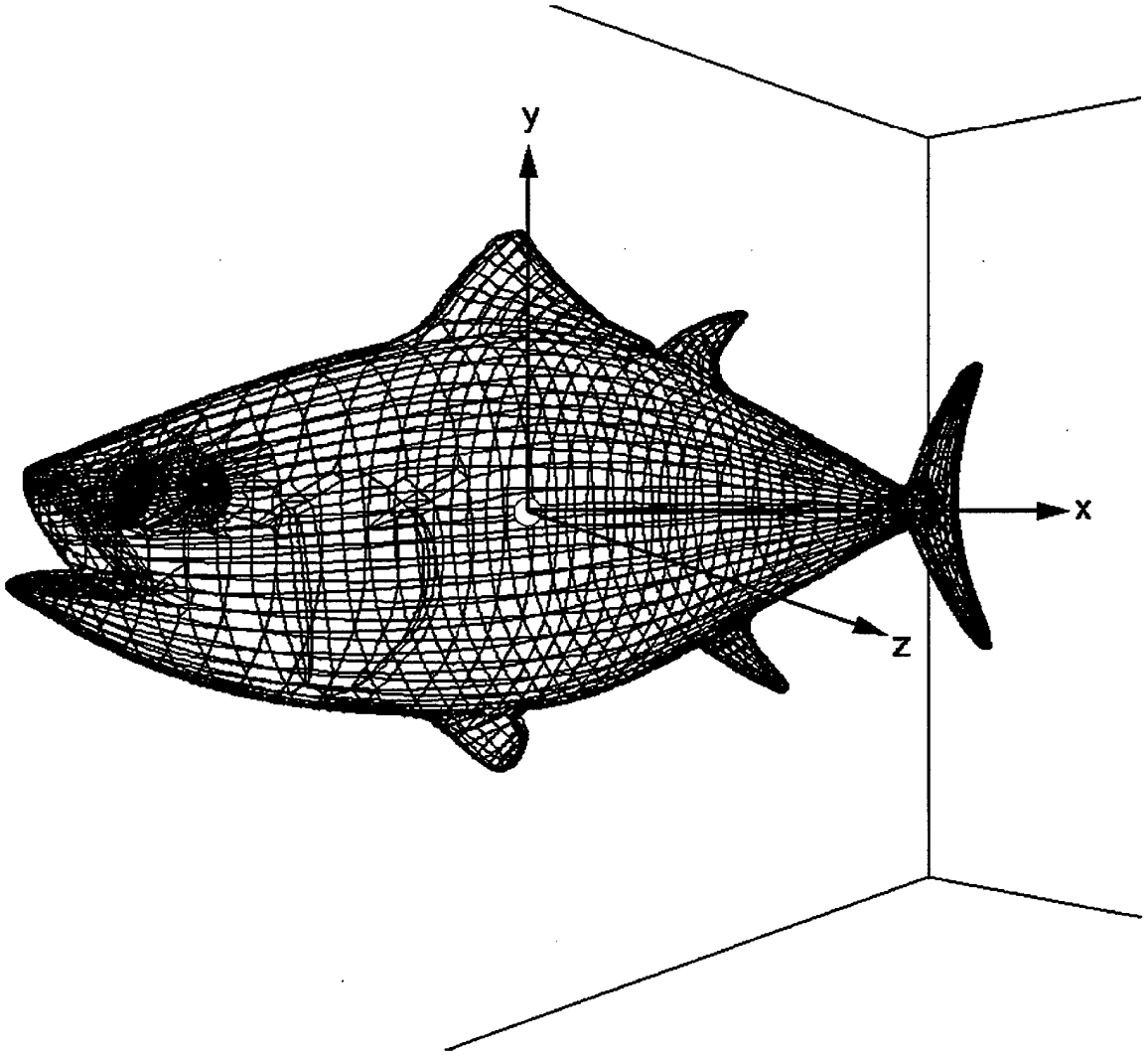

Fig. 5. Surface Definition and Coordinate System

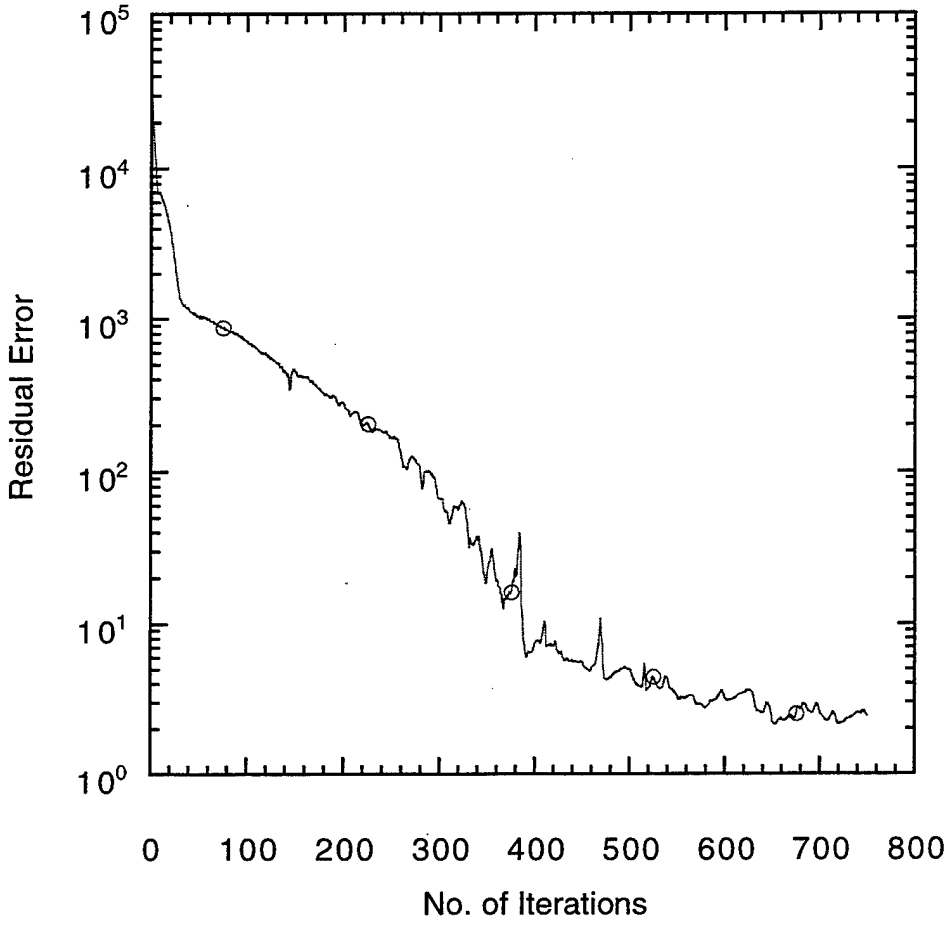

Fig. 6. Convergence History

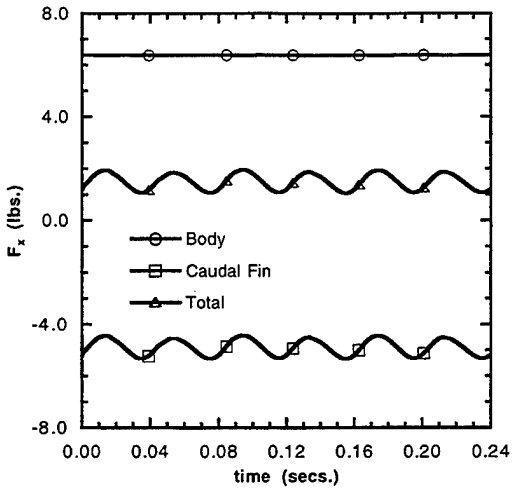

a. x-component

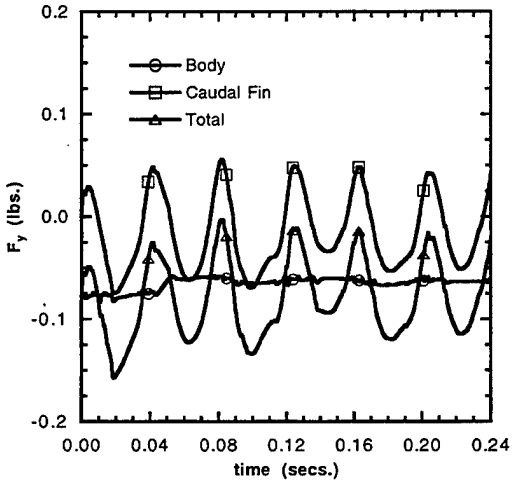

b. y-component

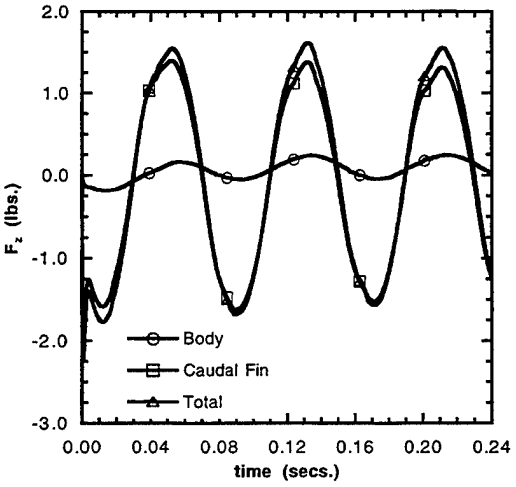

c. z-component

Fig. 7. Time Variation of Force on a Swimming Tuna

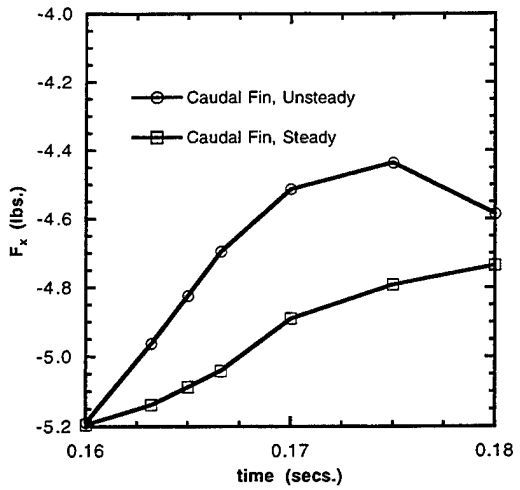

a. x-component

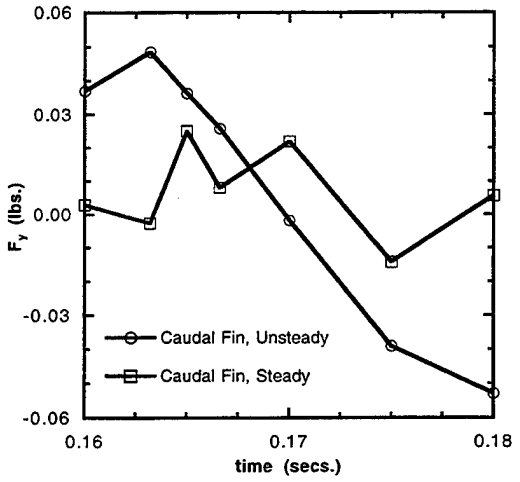

b. y-component

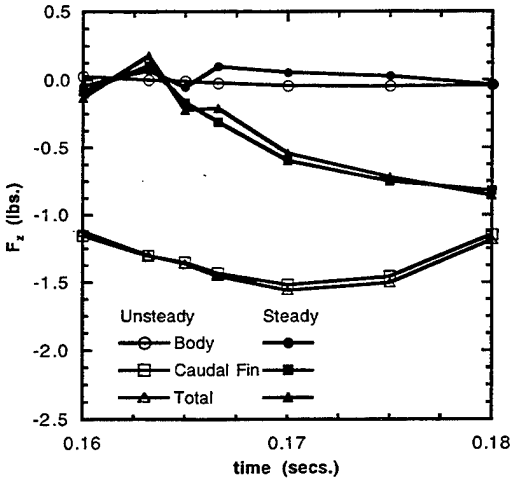

c. z-component

Fig. 8. Effect of Caudal Fin Position on Forces

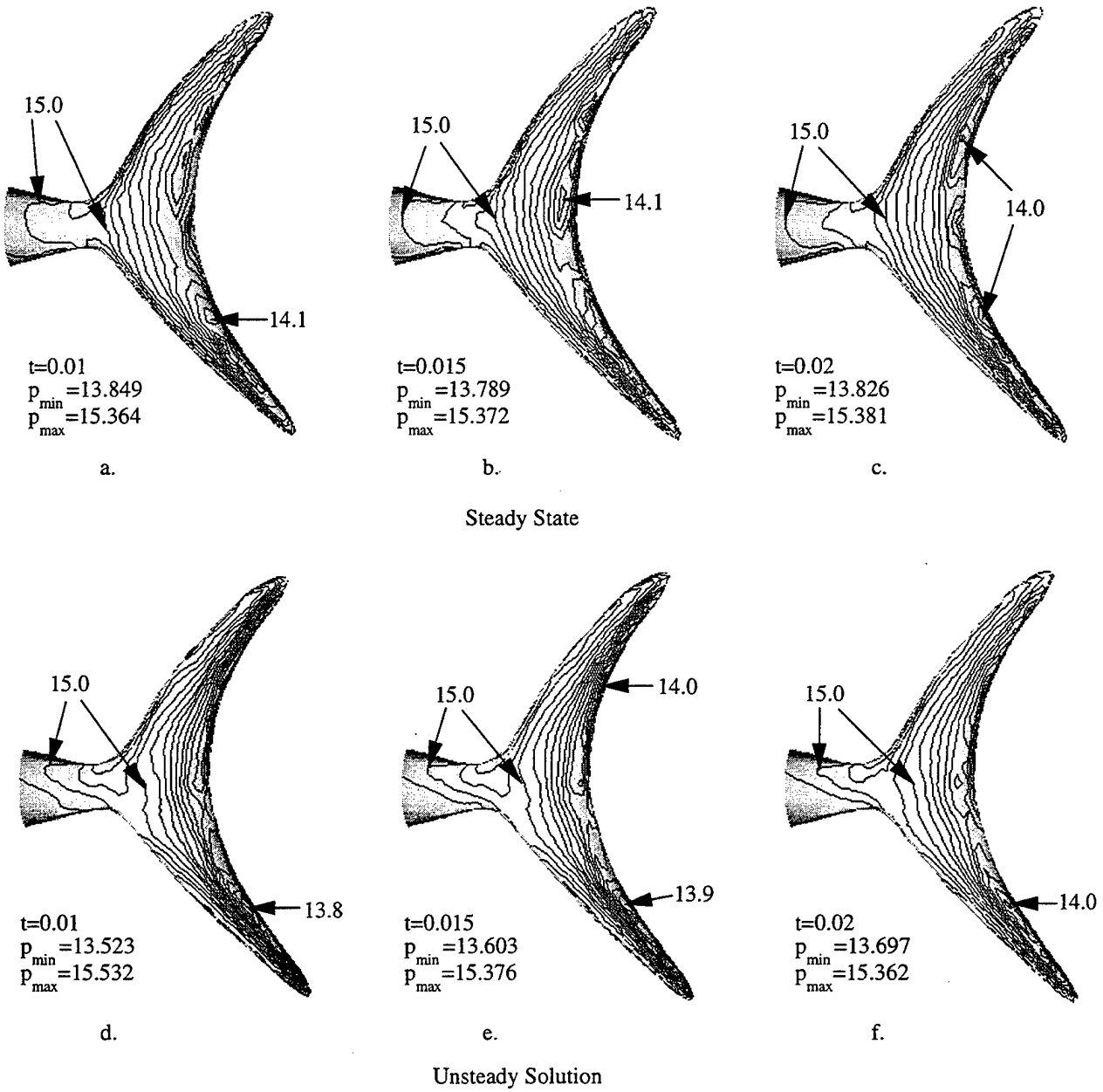

Fig. 9. Comparison of Pressure Distribution on the Pressure Side of the Caudal Fin

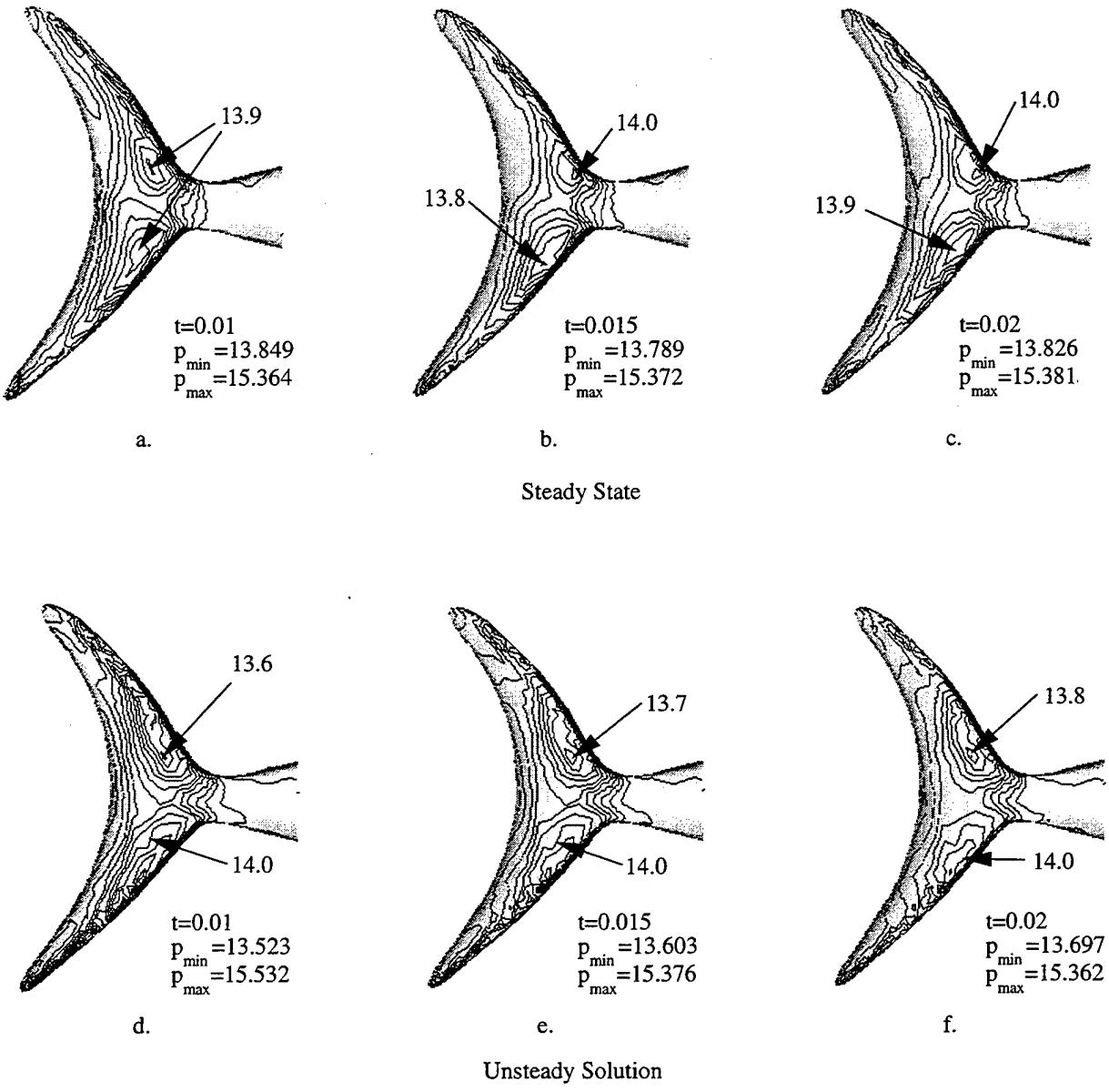

Fig. 10. Comparison of Pressure Distribution on the Suction Side of the Caudal Fin

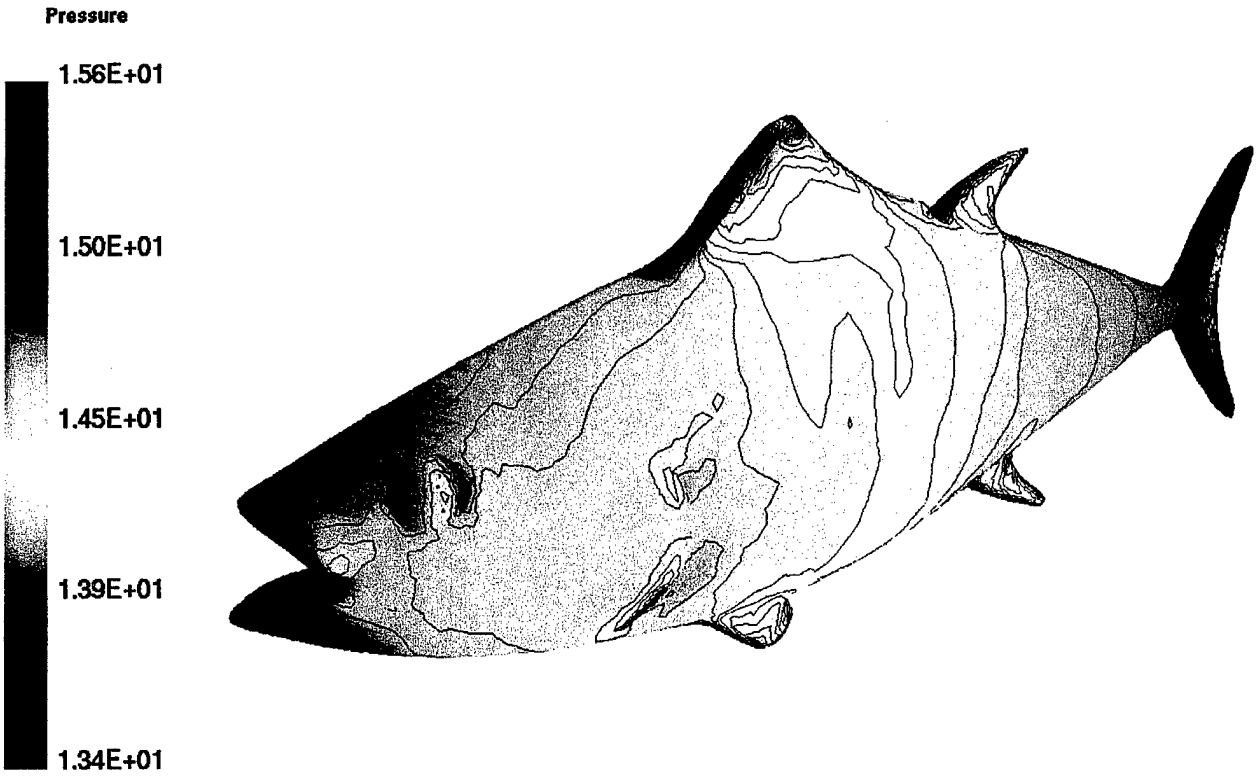

Fig. 11. Surface Pressure Distribution on a Swimming Tuna, t=0.24 Secs

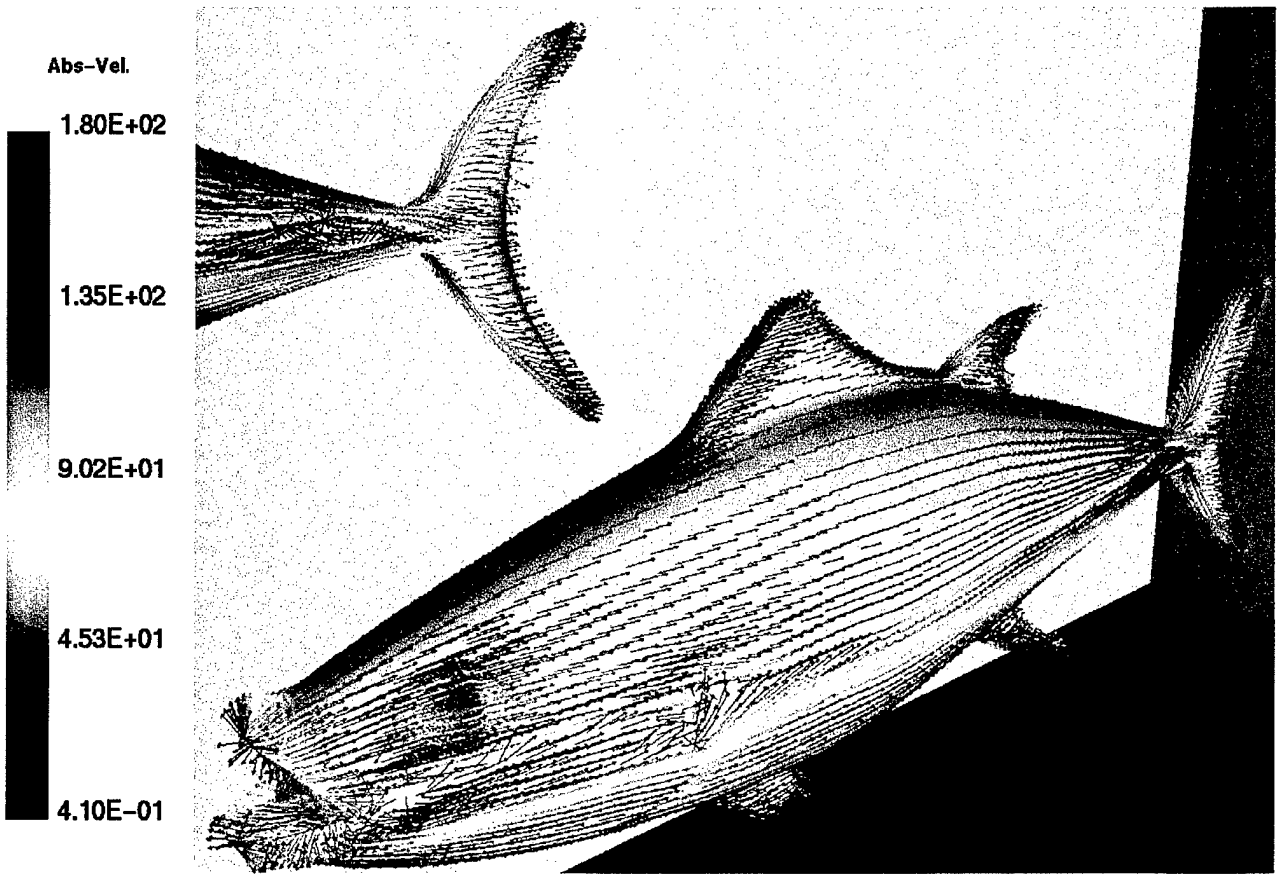

Fig. 12. Velocity Vectors on the Surface of a Swimming Tuna, t=0.24 Secs.

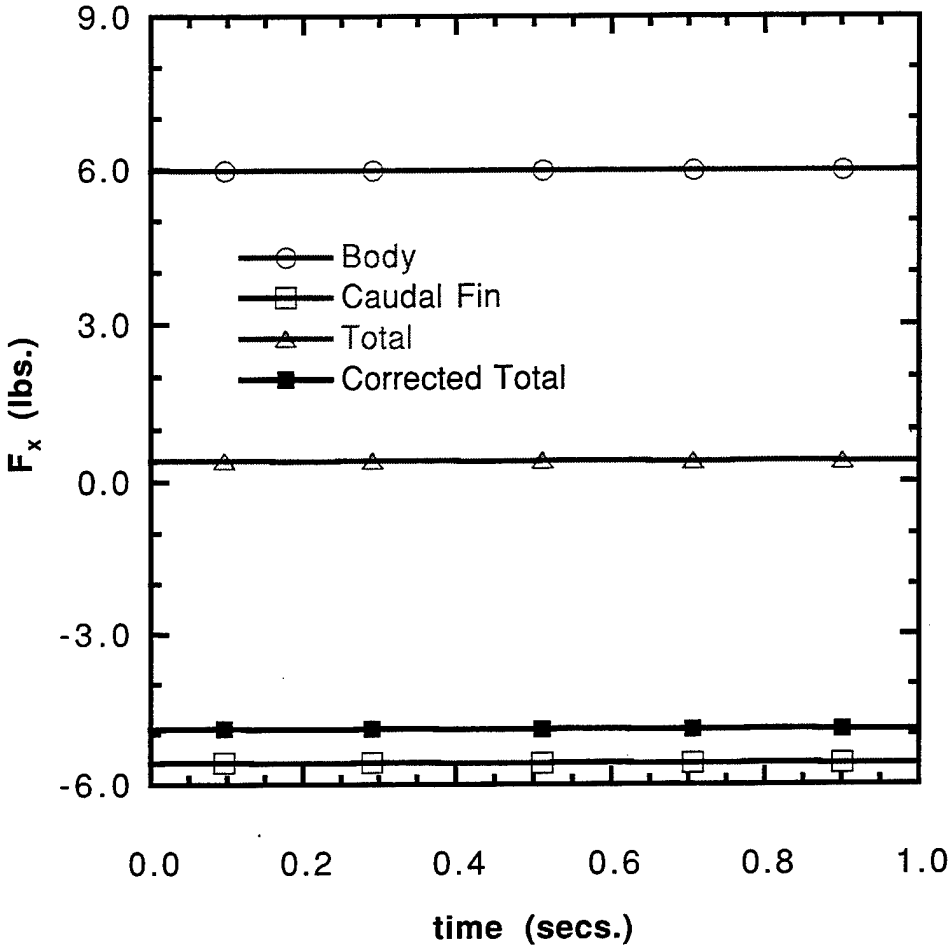

a. x-component

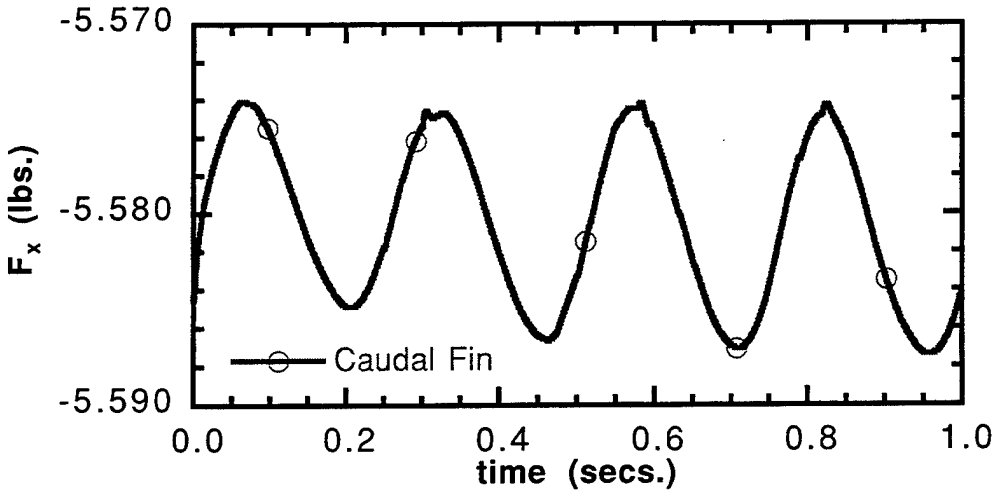

b. Caudal Fin

Fig. 13. Time Variation of Drag Force on a Swimming Tuna for $V = 1\ L/sec.$ and $f_{caudal} = 2\ Hz.$